# Aurora A kinase phosphorylates Hec1 to regulate metaphase kinetochore–microtubule dynamics

Keith F. DeLuca,[1] Amanda Meppelink,[2] Amanda J. Broad,[1] Jeanne E. Mick,[1] Olve B. Peersen,[1] Sibel Pektas,[2] Susanne M.A. Lens,[2] and Jennifer G. DeLuca[1]

[1]Department of Biochemistry and Molecular Biology, Colorado State University, Fort Collins, CO
[2]Oncode Institute, Center for Molecular Medicine, University Medical Center Utrecht, Utrecht, Netherlands

Precise regulation of kinetochore–microtubule attachments is essential for successful chromosome segregation. Central to this regulation is Aurora B kinase, which phosphorylates kinetochore substrates to promote microtubule turnover. A critical target of Aurora B is the N-terminal "tail" domain of Hec1, which is a component of the NDC80 complex, a force-transducing link between kinetochores and microtubules. Although Aurora B is regarded as the "master regulator" of kinetochore–microtubule attachment, other mitotic kinases likely contribute to Hec1 phosphorylation. In this study, we demonstrate that Aurora A kinase regulates kinetochore–microtubule dynamics of metaphase chromosomes, and we identify Hec1 S69, a previously uncharacterized phosphorylation target site in the Hec1 tail, as a critical Aurora A substrate for this regulation. Additionally, we demonstrate that Aurora A kinase associates with inner centromere protein (INCENP) during mitosis and that INCENP is competent to drive accumulation of the kinase to the centromere region of mitotic chromosomes. These findings reveal that both Aurora A and B contribute to kinetochore–microtubule attachment dynamics, and they uncover an unexpected role for Aurora A in late mitosis.

## Introduction

The ability of kinetochores to precisely control their attachment strength to microtubules is an important feature of mitotic chromosome segregation. During early mitosis, attachments are labile to prevent premature kinetochore–microtubule stabilization, whereas during late mitosis, attachments are stable so that forces can be generated for chromosome congression and to silence the spindle assembly checkpoint. Central to this regulation is Aurora B, a mitotic kinase that phosphorylates kinetochore substrates to promote microtubule turnover (Biggins et al., 1999; Tanaka et al., 2002; Lampson et al., 2004; Cheeseman et al., 2006; Cimini et al., 2006; DeLuca et al., 2006; Kelly and Funabiki, 2009). A key Aurora B target involved in this regulation is the Hec1 subunit of the heterotetrameric kinetochore-associated NDC80 complex, which contributes to the formation of stable end-on attachments to spindle microtubules (Cheeseman and Desai, 2008; DeLuca and Musacchio, 2012; Sarangapani and Asbury, 2014). Hec1 is phosphorylated by Aurora B kinase on as many as nine target sites situated within its unstructured "tail" domain, which tunes the affinity of kinetochores for microtubules in cells as well as NDC80 complexes for microtubules in vitro (Cheeseman et al., 2006; DeLuca et al., 2006, 2011; Zaytsev et al., 2014, 2015).

A previous study using phosphospecific antibodies to Aurora B target residues within the Hec1 tail revealed that phosphorylation on all tested sites is high at kinetochores in early mitosis and decreases significantly as cells progress to metaphase (DeLuca et al., 2011). This is consistent with current models for Aurora B–mediated regulation of kinetochore–microtubule attachments, which posit that the kinetochore substrates are either pulled away from Aurora B as a result of centromere and kinetochore stretching upon chromosome biorientation (Liu et al., 2009) or that recruitment of the kinase to kinetochores decreases upon stable microtubule attachment (Caldas et al., 2013). We recently demonstrated that relatively high levels of Hec1 phosphorylation are required for dynamic kinetochore–microtubule attachments during prometaphase that facilitate error correction and that low but sustained levels of phosphorylation are required for kinetochore–microtubule dynamics that facilitate chromosome movements during metaphase (Zaytsev et al., 2014). In this study, we set out to investigate whether any uncharacterized phosphorylation sites in the Hec1 tail might contribute to these sustained low levels of phosphorylation in metaphase. We demonstrate that phosphorylation dynamics of serine 69 (S69) differ significantly from previously characterized tail domain target sites (DeLuca et al., 2011). S69 remains highly phosphorylated in metaphase, and preventing phosphorylation of S69 impairs metaphase kinetochore–microtubule dynamics. Inhibitor treatment reveals that this site is primarily phosphorylated by Aurora A kinase, a well-characterized spindle pole–associated kinase (Ducat and Zheng, 2004; Barr

Correspondence to Jennifer G. DeLuca: jdeluca@colostate.edu; Susanne M.A. Lens: s.m.a.lens@umcutrecht.nl

and Gergely, 2007), rather than Aurora B kinase. Furthermore, we find that Aurora A not only contributes to kinetochore phosphorylation of Hec1 on pole-proximal chromosomes in early mitosis, but surprisingly, Aurora A kinase activity is required for sustained phosphorylation on S69 throughout the duration of mitosis and for the regulation of kinetochore–microtubules of aligned metaphase chromosomes. Finally, we demonstrate that Aurora A associates with inner centromere protein (INCENP) in mitotic cells and that INCENP can drive Aurora A localization to centromeres, which may explain the sustained S69 phosphorylation on metaphase chromosomes.

## Results

Based on our previous results demonstrating that low but sustained levels of phosphorylation on the Hec1 tail are required for proper kinetochore–microtubule dynamics during metaphase, we hypothesized that phosphorylation of uncharacterized sites might contribute to this metaphase function (Zaytsev et al., 2014). To test this, we generated antibodies against a previously untested phosphorylated residue in the Hec1 tail, S69 (Fig. 1, A and B; and Fig. S1, A and B), and determined its kinetochore localization pattern during mitosis. Similar to sites that we previously tested (DeLuca et al., 2011), S69 was phosphorylated in early mitosis; however, in contrast to the other phospho sites, S69 remained highly phosphorylated throughout all stages of mitosis in both HeLa and PtK1 cells, and levels remained constant from prometaphase to metaphase (Figs. 1 C and S1 B). Consistent with this result, we observed that the level of S69 phosphorylation on kinetochores of aligned and unaligned chromosomes in individual cells was similar (Fig. 1 D). To quantify this effect, we enriched for cells with pole-proximal chromosomes by depleting the plus end–directed microtubule motor protein CENP-E (Schaar et al., 1997; Wood et al., 1997) and measured pS69 levels on aligned and pole-proximal kinetochores. Kinetochore-associated pS69 levels were similar between both kinetochore populations (Fig. 1 E). This is in contrast to pS55 and pS44, whose levels were high on kinetochores of pole-proximal chromosomes but low on kinetochores of aligned chromosomes (Fig. 1 E; DeLuca et al., 2011).

To investigate the role of microtubule attachment status and dynamics in S69 phosphorylation, we treated cells with 1 µM nocodazole (to destabilize spindle microtubules), 10 µM taxol (to promote microtubule polymerization), or 50 nM taxol (to dampen microtubule dynamics; Jordan et al., 1992, 1993; Derry et al., 1995). Kinetochore–microtubule attachment status after drug treatments was determined by staining cells for Mad2 (Fig. S1 C). Treatment of cells with either 10 µM or 50 nM taxol did not alter kinetochore Hec1 S69 phosphorylation levels (Fig. 2, A and B). However, cells treated with 1 µM nocodazole exhibited significantly decreased levels of S69 phosphorylation at kinetochores (Fig. 2 C), suggesting that microtubules promote phosphorylation at this site.

We next tested whether phosphorylation of S69 was dependent on Aurora B kinase, which is the case for other sites within the Hec1 tail domain (DeLuca et al., 2011). Although Aurora B was able to phosphorylate S69 in vitro (Fig. 4; DeLuca et al., 2006), kinetochores in cells treated with an Aurora B inhibitor, ZM447439, exhibited only a modest reduction in S69 phosphorylation, whereas S55 phosphorylation was substantially decreased after Aurora B inhibition, and S44

phosphorylation was nearly abolished (Fig. 3, A and B). Aurora B kinase shares a nearly identical consensus phosphorylation sequence with Aurora A kinase (Kettenbach et al., 2011), and it has been suggested that substrate specificity of these two kinases is largely governed by their subcellular localization, with Aurora B and its substrates residing at the centromere and kinetochore in mitosis, and Aurora A and its substrates residing at the spindle poles (Hans et al., 2009; Hochegger et al., 2013; Li et al., 2015). Given the similarity in consensus sequences, we tested whether Aurora A contributes to Hec1 phosphorylation in cells. Interestingly, inhibition of Aurora A with MLN8054 (Hoar et al., 2007; Manfredi et al., 2007) had differential effects on phosphorylation of target sites within the Hec1 tail domain. Specifically, S69 phosphorylation was reduced to a greater extent after inhibitor treatment compared with S55 and even more so compared with S44 (Fig. 3, A and B). Treatment of cells with both Aurora B and Aurora A inhibitors resulted in a nearly complete loss of phosphostaining for all Hec1 sites tested (Fig. 3, A and B). These results suggest that Aurora A kinase, rather than Aurora B, is primarily responsible for phosphorylation of Hec1 S69. In addition, they suggest that S44 is primarily phosphorylated by Aurora B and that S55 is phosphorylated by both kinases. This latter finding is consistent with two recent studies demonstrating that in early mitosis, spindle pole–localized Aurora A contributes to the phosphorylation of S55 (Chmátal et al., 2015; Ye et al., 2015). Given the role of microtubules in promoting Aurora A activity (Silva and Cassimeris, 2013), this may explain our earlier result that cells treated with 1 µM nocodazole exhibited reduced S69 phosphorylation at kinetochores (Fig. 2, C and D). Importantly, we ensured that the concentrations of Aurora A and Aurora B inhibitors used (Aurora A, 0.5 µM MLN8054 in HeLa cells and 1 µM MLN8054 in PtK1 cells; Aurora B, 2 µM ZM447439 for both HeLa and PtK1 cells) had minimal effects on the activity of Aurora B and Aurora A, respectively. (Figs. 3 C and S2).

The differential effects of Aurora B and Aurora A inhibition on phosphorylation target sites in the Hec1 tail suggested that the two kinases might exhibit varying degrees of specificity toward different sites. We tested this by carrying out Aurora A and B in vitro kinase assays using increasing concentrations of purified NDC80$^{Bonsai}$ (Ciferri et al., 2008) as a substrate (Fig. 4). As shown in Fig. 4, Aurora A and Aurora B were able to phosphorylate all Hec1 sites tested, and the amount of substrate required for half-maximal phosphorylation differed only modestly between individual phospho sites for each kinase (Fig. 4). These results suggest that although the two kinases may exhibit a low level of inherent specificity for individual sites within the Hec1 tail, the differences observed at kinetochores are likely influenced primarily by cellular context. We reasoned that a contributing factor to the differences in activity toward different sites within the tail domain in cells might be substrate accessibility—it is possible that the location in the tail region may affect a particular sites' ability to be accessed by either Aurora A or Aurora B. To test this possibility, we designed a mutant version of Hec1 in which amino acids 1–56 were swapped with amino acids 57–80 such that the small region containing S69 was moved to the far N terminus of the Hec1 tail, distal from the globular calponin homology domain (Fig. S3 A). We then tested the temporal phosphorylation pattern of S69 and its sensitivity to ZM447439 and MLN8054. Interestingly, shifting the location of S69 did not affect either its temporal pattern of phosphorylation or its sensitivity to Aurora kinase inhibitors (Fig. S3, B and C). These
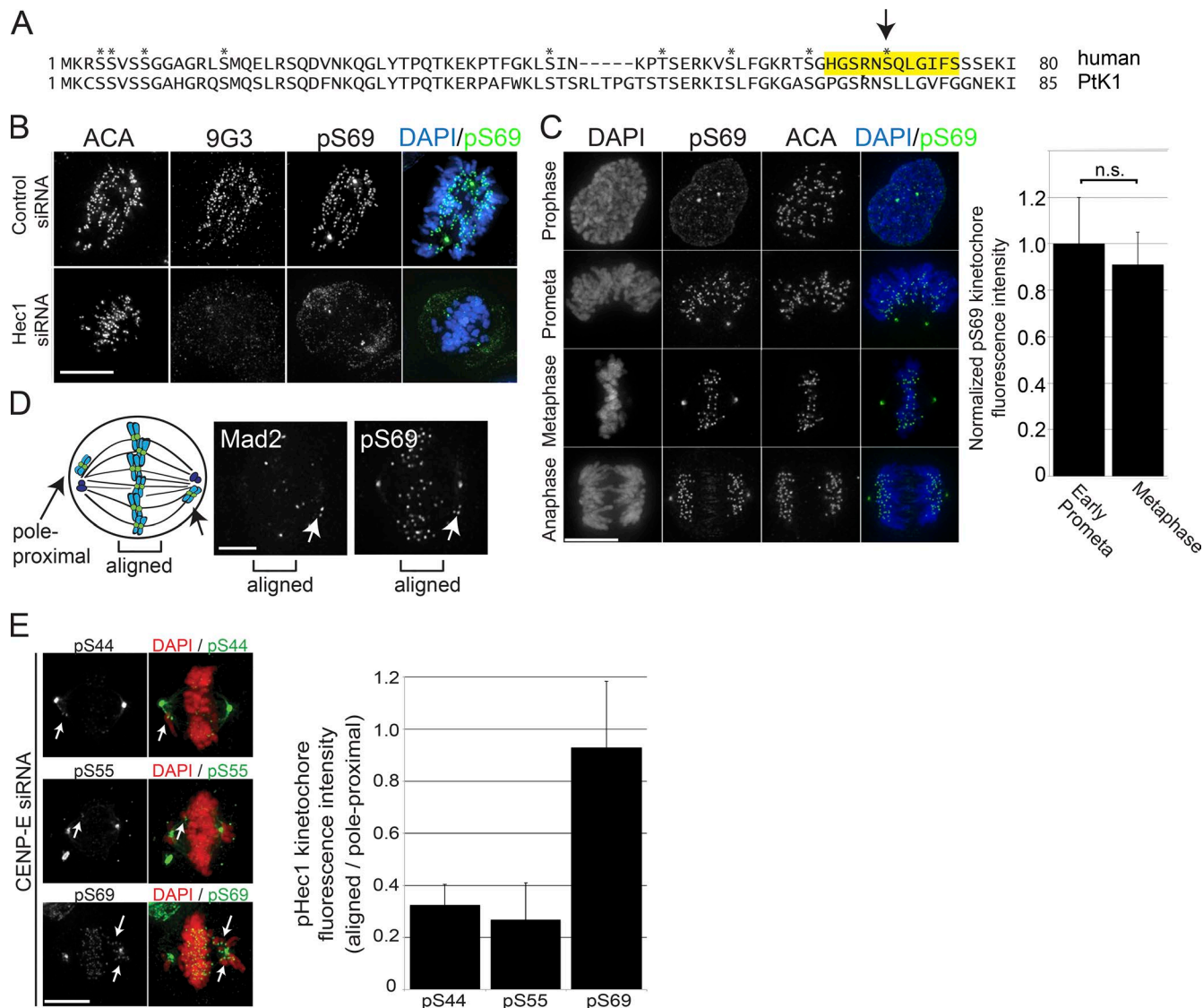
**Figure 1. Hec1 S69 is phosphorylated throughout mitosis. (A)** Amino acid sequences of the human and PtK1 cell (Guimaraes et al., 2008) Hec1 N-terminal tail domain. Shown in yellow is the human peptide sequence that was used to generate the S69 phosphospecific antibody. The arrow points to S69 in the human sequence and the corresponding serine residue in the PtK1 sequence. Asterisks indicate all other mapped Aurora B kinase sites in the human Hec1 tail domain (Cheeseman et al., 2006; DeLuca et al., 2006). **(B)** Immunofluorescence images of HeLa cells stained with phosphospecific antibodies to Hec1 pS69. Depletion of Hec1 (bottom) results in loss of pS69 staining at kinetochores. Cells are also immunostained with antibody 9G3 (pan-Hec1 antibody) and an anticentromere antibody (ACA) derived from human calcinosis, Raynaud's phenomenon, esophageal dysmotility, sclerodactyly, and telangiectasia (CREST) patient serum. **(C)** Immunofluorescence images of HeLa cells demonstrating kinetochore localization of pS69 during mitosis. Quantification is shown on the right. For each phase shown, ≥400 kinetochores from ≥30 cells were measured. **(D)** Immunofluorescence images of a HeLa cell stained with antibodies to pS69 and Mad2. For the cell shown, most chromosomes are aligned at the spindle equator, and one chromosome remains near a spindle pole (arrows). A schematic illustrating examples of pole-proximal chromosomes is shown on the left. **(E)** Immunofluorescence images of HeLa cells depleted of CENP-E to increase the number of pole-proximal chromosomes (arrows) and stained with Hec1 phosphospecific antibodies. Quantification is shown on the right from one representative experiment. *n* values are as follows: pS69, 20 polar kinetochores and 40 aligned kinetochores; pS55, 17 polar kinetochores and 57 aligned kinetochores; and pS44, 13 polar kinetochores and 29 aligned kinetochores. Error bars indicate SD. Bars: (B, C, and E) 10 µm; (D) 3 µm.

results suggest the presence of other cellular influences on kinase specificity for particular tail domain target sites. It is also possible that dephosphorylation of individual phospho sites may be differentially regulated, which we did not explore in this study.

The persistent phosphorylation of S69 in metaphase suggested that this modification might be important for late mitotic kinetochore function. To determine whether phosphorylation of S69 is required for normal metaphase kinetochore–microtubule dynamics, we expressed a nonphosphorylatable S69 mutant (S69A-Hec1-GFP) in PtK1 cells depleted of endogenous Hec1 and tracked kinetochore oscillatory movements in metaphase.

From the tracking data, we calculated the deviation from average position (Stumpff et al., 2008) of each kinetochore to gauge oscillation amplitude. Antibody staining of S69A-Hec1-GFP–transfected cells confirmed that the mutant-expressing cells were not phosphorylated at S69 (Fig. S4 A). Indeed, metaphase kinetochore oscillations in cells expressing S69A-Hec1-GFP but not S44A-Hec1-GFP or S55A-Hec1-GFP were significantly dampened when compared with cells expressing WT-Hec1-GFP (Fig. 5 A), suggesting that Aurora A–mediated phosphorylation of this site contributes to proper kinetochore–microtubule dynamics in late mitosis.
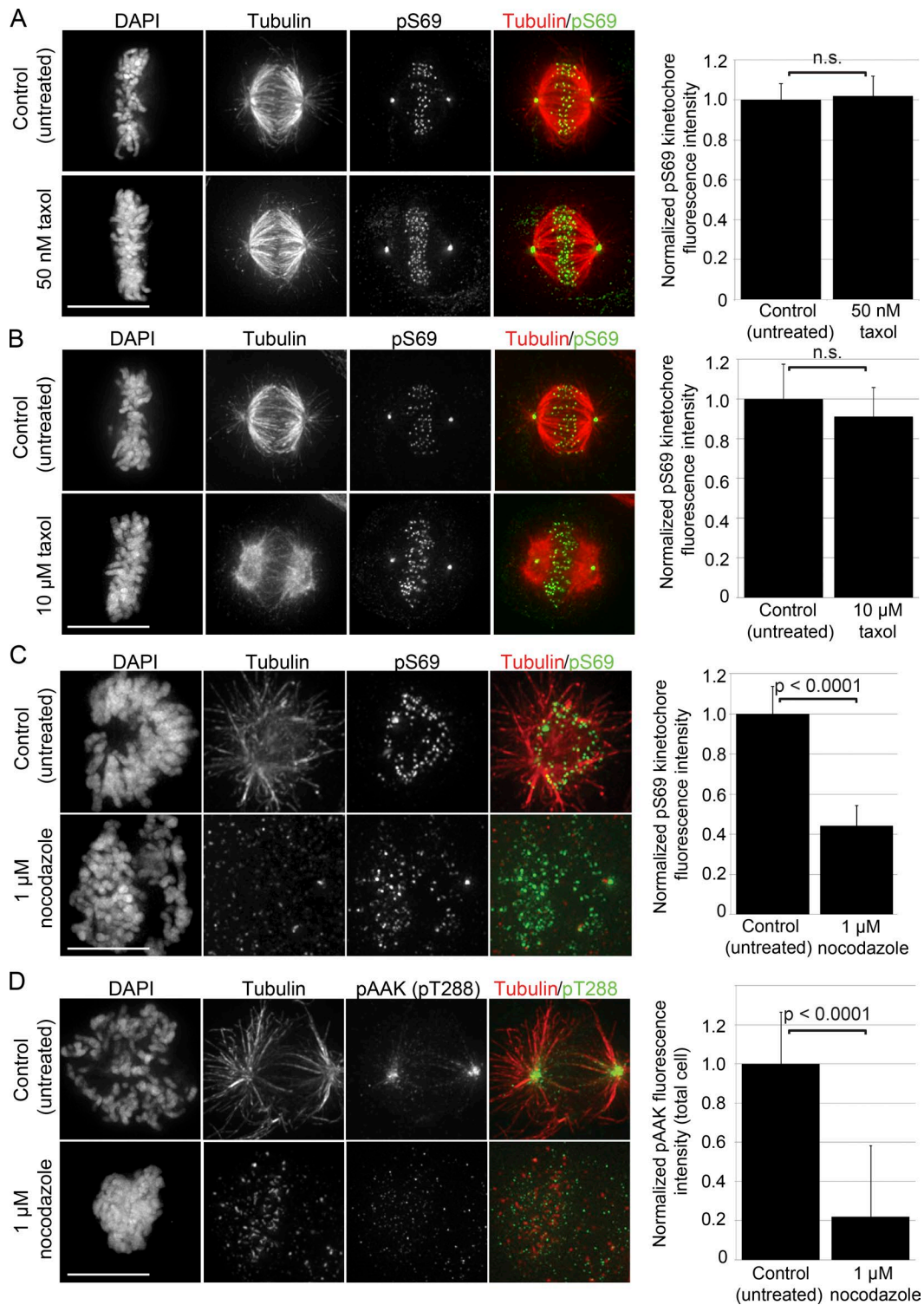
Figure 2. **Hec1 S69 phosphorylation is reduced at kinetochores in response to microtubule depolymerization but not in response to microtubule stabilization. (A–C)** Immunofluorescence images showing kinetochore localization of pS69 in HeLa cells after incubation with 50 nM taxol for 5 h (A), 10 µM taxol for 30 min (B), and 1 µM nocodazole for 1 h (C). **(D)** Immunofluorescence images of control cells and cells treated with 1 µM nocodazole for 1 h and stained with an antibody to active Aurora A kinase phosphorylated at T288 (pT288). Shown on the right of each panel is the quantification of either pS69 kinetochore fluorescence intensity (A–C) or total cellular pAAK fluorescence intensity (D). For all conditions in A–C, ≥200 kinetochores were measured from ≥20 cells. For the experiment shown in D, total fluorescence was measured from ≥20 cells per condition. Error bars indicate SD. Bars, 10 µm.

Because Aurora A is a well-characterized spindle pole–associated kinase, it is reasonable to assume that the observed MLN8054-induced reduction in S69 phosphorylation is a consequence of decreased spindle pole–associated Aurora A kinase activity (Kunitoku et al., 2003; Ducat and Zheng, 2004; Barr and Gergely, 2007; Kim et al., 2010; Chmátal et al., 2015; Ye et al., 2015). We therefore hypothesized that Aurora A phosphorylates S69 in early mitosis when kinetochores of unaligned
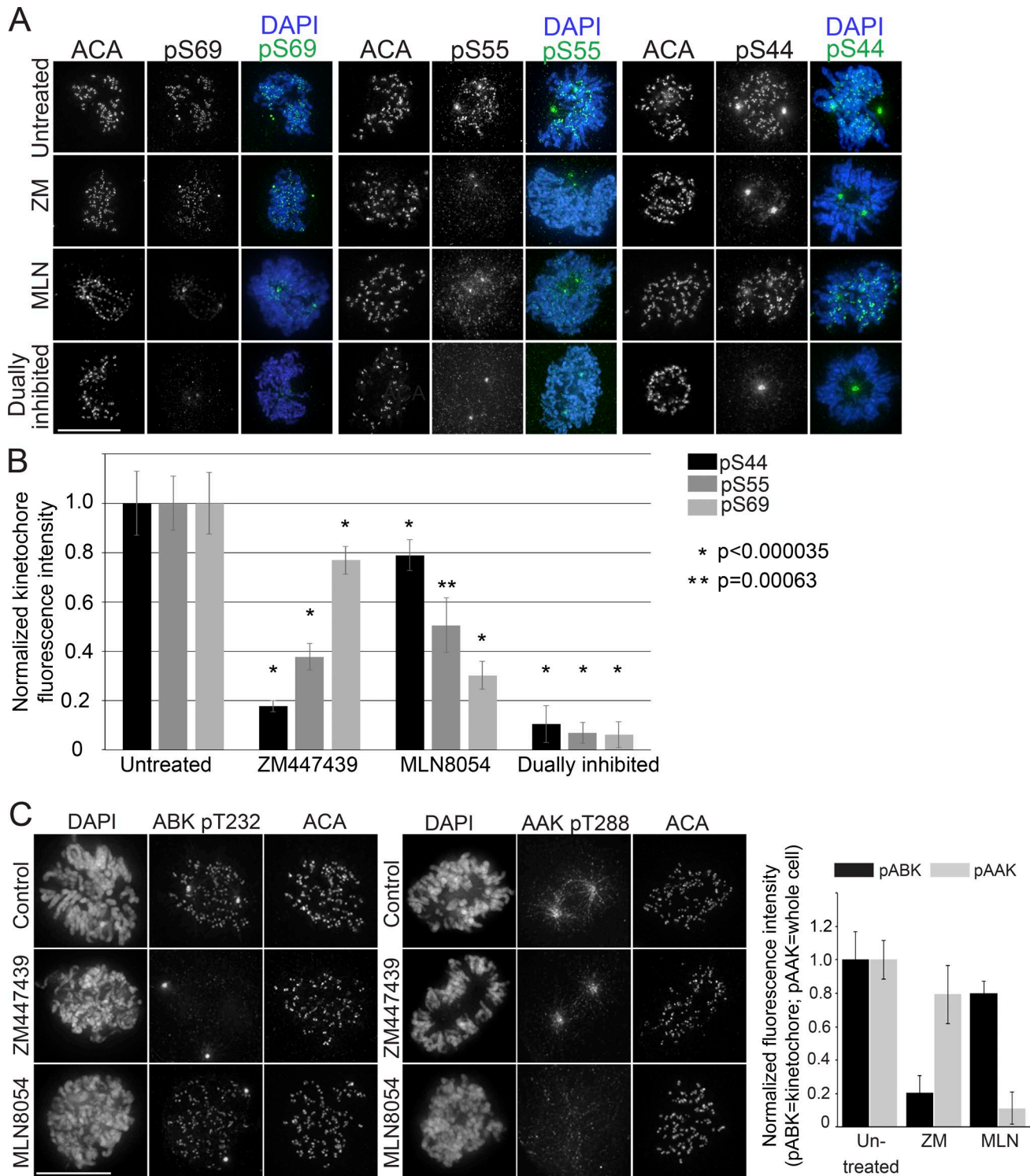
Figure 3. **Hec1 S69 is phosphorylated by Aurora A kinase in cells. (A)** Immunofluorescence images of HeLa cells treated with 2 µM ZM447439 (ZM) to inhibit Aurora B kinase (ABK), 0.5 µM MLN8054 (MLN) to inhibit Aurora A kinase (AAK), or both inhibitors, and stained with phosphospecific antibodies to Hec1 S69, S55, and S44. **(B)** Quantification of the experiment represented in A. For each condition, ≥300 kinetochores were measured from ≥30 cells. Asterisks indicate respective p-values (each condition is compared with the corresponding untreated control; unpaired *t* test). **(C)** Fluorescence images showing cells immunostained with antibodies to active Aurora B kinase phosphorylated at T232 (pT232) and active Aurora A kinase phosphorylated at T288 (pT288) in HeLa cells treated with either 0.5 µM MLN8054, 2 µM ZM447439, or no inhibitor. Quantification is shown on the right. For each condition shown, ≥300 kinetochores from ≥30 cells were measured. Error bars indicate SD. Bars, 10 µm. ACA, anticentromere antibody.

chromosomes are likely to reside near a spindle pole (Kuni-toku et al., 2003; Kim et al., 2010; Chmátal et al., 2015; Ye et al., 2015). In this scenario, high levels of S69 phosphorylation

persist from early prometaphase through metaphase, and this sustained phosphorylation mediates proper kinetochore–microtubule dynamics at metaphase. To test this, we allowed
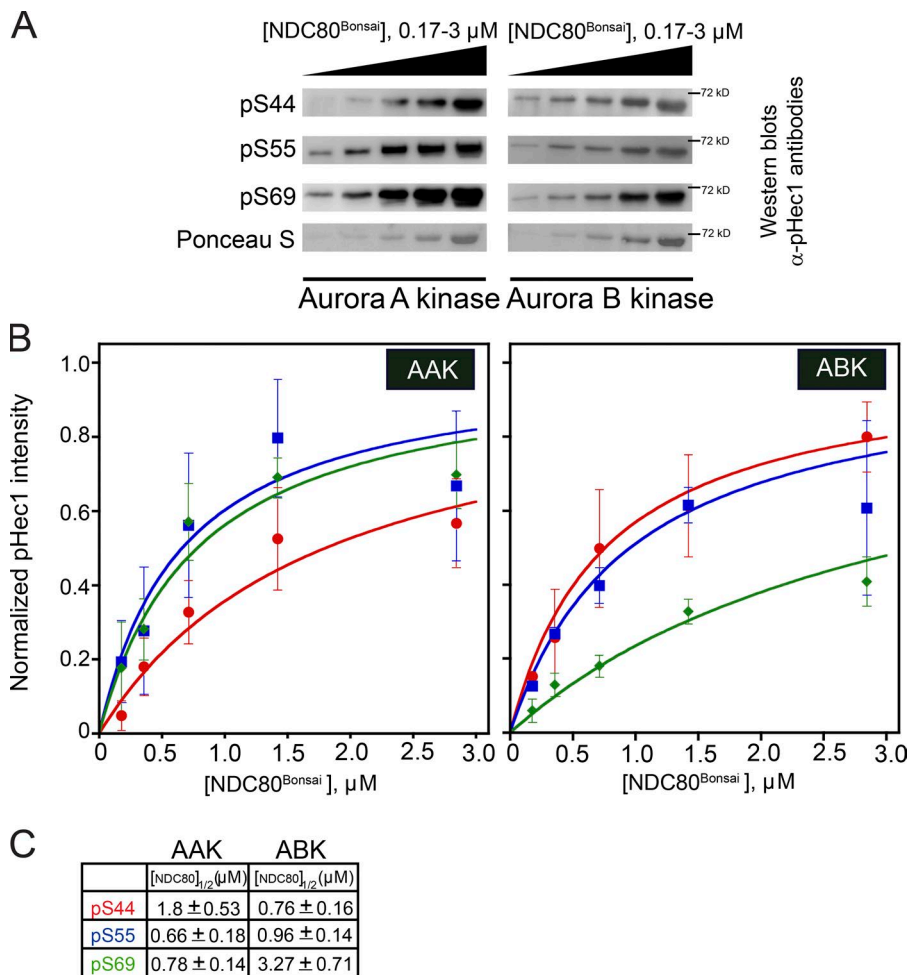
A
[NDC80^Bonsai], 0.17-3 µM    [NDC80^Bonsai], 0.17-3 µM

pS44 — 72 kD
pS55 — 72 kD
pS69 — 72 kD
Ponceau S — 72 kD

Western blots α-pHec1 antibodies

Aurora A kinase    Aurora B kinase

B

AAK    ABK
Normalized pHec1 intensity vs [NDC80^Bonsai], µM

C

| | AAK | ABK |
| | [NDC80]$_{1/2}$ (µM) | [NDC80]$_{1/2}$ (µM) |
|---|---|---|
| pS44 | 1.8 ± 0.53 | 0.76 ± 0.16 |
| pS55 | 0.66 ± 0.18 | 0.96 ± 0.14 |
| pS69 | 0.78 ± 0.14 | 3.27 ± 0.71 |

Figure 4. **Aurora A and Aurora B kinases phosphorylate Hec1 target residues with similar efficiencies in vitro.** (A) Purified NDC80^Bonsai complexes (Ciferri et al., 2008) were subjected to in vitro phosphorylation by Aurora A kinase (AAK) or Aurora B kinase (ABK) under conditions of increasing substrate concentration. Reactions were subjected to SDS-PAGE and Western blot analysis. Western blots of purified NDC80^Bonsai complexes were probed with phosphospecific Hec1 antibodies or Ponceau S. (B) Curve fits for the substrate titration experiment were performed; concentration of substrate (NDC80^Bonsai) is plotted on the x axis, and normalized pHec1 intensity is plotted on the y axis. For each curve, three to five independent experiments were performed using five concentrations of NDC80^Bonsai substrate. Error bars indicate SD. (C) Calculated values for the concentration of NDC80^Bonsai required for half maximal phosphorylation at each site (S44, S55, or S69) by Aurora A and Aurora B kinases.

mitotic cells to progress to metaphase, added MLN8054 only after all chromosomes were aligned at the spindle equator, and subsequently fixed and immunostained cells using pS69 antibodies. This experiment revealed, counter to our prediction, a significant decrease in S69 phosphorylation at kinetochores (Fig. 5 B), indicating that sustained Aurora A kinase activity in metaphase is required to maintain S69 in a phosphorylated state. Consistently, MLN8054 treatment of those metaphase cells in which chromosomes were fully aligned nearly eliminated kinetochore oscillations (Fig. 5 C). Collectively, these results suggest that sustained activity of Aurora A near kinetochores (i.e., distal from the spindle poles) is required for normal kinetochore–microtubule regulation in metaphase. Cells with fully aligned chromosomes treated with ZM447439, however, retained high levels of phosphorylated S69 and exhibited only modest changes in kinetochore oscillations (Fig. 5, B and C). In contrast, it is well established that treating early mitotic cells with the Aurora B inhibitor ZM447439 results in severe defects in kinetochore–microtubule attachment regulation, dampened kinetochore movements, and gross chromosome segregation errors (Kallio et al., 2002; Ditchfield et al., 2003; Hauf et al., 2003; Cimini et al., 2006), consistent with a role for Aurora B in promoting kinetochore–microtubule turnover to facilitate attachment error correction in early mitosis.

To determine whether the defects in metaphase kinetochore oscillations in response to Aurora A inhibition were caused by loss of Hec1 phosphorylation and not by perturbation of other mitotic Aurora A functions, we generated a mutant

version of Hec1 in which S69 was mutated to aspartic acid to mimic constitutive phosphorylation, and the remaining eight phosphorylation target sites were mutated to alanine to prevent phosphorylation (8A-S69D-Hec1-GFP; Zaytsev et al., 2014). Cells expressing the single aspartic acid substitution mutant exhibited significantly increased kinetochore oscillations in the presence of MLN8054 when compared with cells expressing WT-Hec1-GFP treated with MLN8054 (Fig. 5 D), which suggests that Hec1 is a key target of Aurora A that facilitates late mitotic kinetochore function. We additionally tested a mutant in which S55 was replaced with an aspartic acid (8A-S55D-Hec1-GFP) and found that this mutant also rescued kinetochore oscillations in the presence of MLN8054, consistent with our previously published results that a single phosphomimetic substitution at any site in the Hec1 tail facilitates metaphase kinetochore oscillations (Zaytsev et al., 2014). However, of all Hec1 tail domain phosphorylation target sites tested to date, only S69 is highly phosphorylated in late mitosis; thus, this residue is likely the physiological Aurora A target that promotes kinetochore–microtubule dynamics at metaphase.

To test this hypothesis, we transfected cells with Hec1 mutants in which eight of the nine mapped Aurora kinase tail domain target sites were mutated to alanine (to prevent phosphorylation), and one site was left in its WT state (e.g., 8A-S69^WT-Hec1-GFP). We first ensured that the available WT sites were able to be phosphorylated in the context of an otherwise nonphosphorylatable tail domain by immunostaining fixed cells with the corresponding phosphospecific antibody (Fig. S4
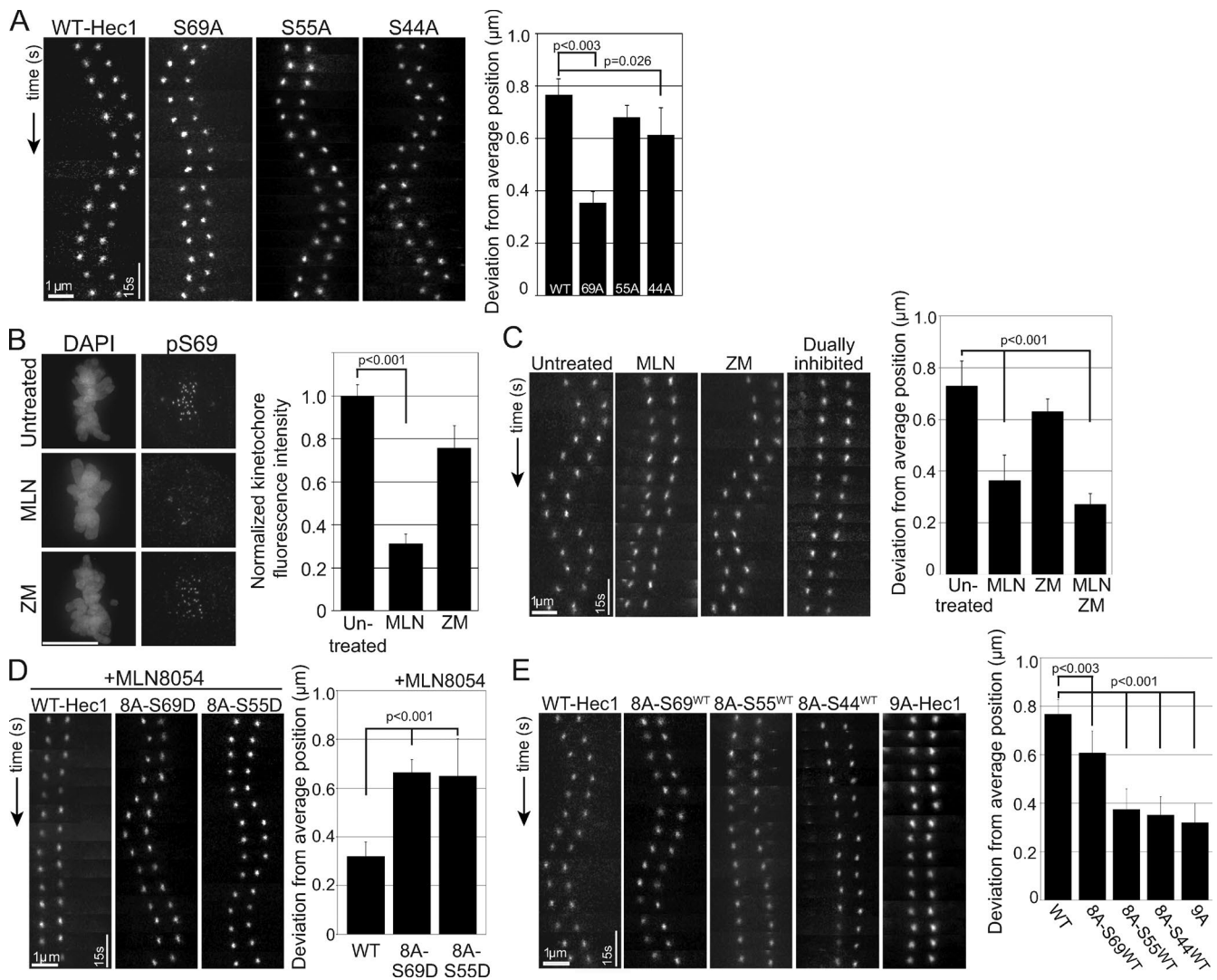
Figure 5. **Aurora A kinase phosphorylation of Hec1 S69 is required for metaphase kinetochore function. (A)** Kymographs of individual sister kinetochore pairs from live-cell time-lapse imaging sequences of PtK1 cells depleted of endogenous Hec1 and rescued with WT-Hec1-GFP (WT) or mutants of Hec1 with a single phosphorylation site mutated to alanine: S69A, S55A, and S44A. Cells were treated with 10 μM MG132 before imaging. Quantification of the deviation from average position (Stumpff et al., 2008) is shown on the right. For each condition, ≥30 kinetochore pairs from a total of nine cells were analyzed. **(B)** Immunofluorescence images of untreated PtK1 cells or cells treated with 1 μM MLN8054 (MLN) or 2 μM ZM447439 (ZM). All cells were additionally treated with 10 μM MG132 at the time of kinase inhibitor addition. After 1 h, cells were fixed and stained with antibodies to phosphorylated S69 (pS69). Bar, 10 μm. Shown on the right is the quantification of pS69 kinetochore fluorescence intensity. For each condition, ≥200 kinetochores were measured from ≥20 cells. **(C)** Kymographs of individual sister kinetochore pairs from live-cell time-lapse imaging sequences of untreated PtK1 cells or cells treated with 1 μM MLN8054, 2 μM ZM447439, or both inhibitors. All cells were treated with 10 μM MG132 at the time of inhibitor addition. Quantification of the deviation from average position is shown on the right. For each condition, ≥20 kinetochore pairs were measured from at least five cells. **(D)** Kymographs of individual sister kinetochore pairs from live-cell time-lapse imaging sequences of PtK1 cells depleted of endogenous Hec1 and rescued with WT-Hec1-GFP or mutants of Hec1 with either S69 or S55 mutated to aspartic acid and the eight remaining phosphorylation target sites mutated to alanine (e.g., 8A-S69D-Hec1-GFP). Cells were treated with 1 μM MLN8054 and 10 μM MG132 before imaging. Quantification of the deviation from average position is shown on the right. For each condition, ≥20 kinetochore pairs were measured from at least five cells. **(E)** Kymographs of individual sister kinetochore pairs from live-cell time-lapse imaging sequences of PtK1 cells depleted of endogenous Hec1 and rescued with WT-Hec1-GFP, 9A-Hec1-GFP, or mutants of Hec1 with all phosphorylation target sites except for one (S69, S55, or S44) mutated to alanine. The remaining site was left as an unperturbed serine (e.g., 8A-S69WT-Hec1-GFP). Quantification of the deviation from average position is shown on the right. For each condition, ≥20 kinetochore pairs were measured from at least five cells. For all kymographs, distance scale bars are 1 μm, and time scale bars are 15 s. Error bars indicate SD. All kymographs represent individual sister kinetochore pairs displayed over time.

B). We then tracked the movements of kinetochores of aligned chromosomes in cells depleted of endogenous Hec1 and expressing the mutant versions. As expected, kinetochores in cells transfected with 9A-Hec1-GFP (all mapped sites including S69 mutated to alanine) failed to oscillate normally (Fig. 5 E). However, cells expressing 8A-S69WT-Hec1-GFP but not 8A-S44WT-Hec1-GFP or 8A-S55WT-Hec1-GFP exhibited increased kinetochore oscillations over those observed in 9A-expressing cells (Fig. 5 E), demonstrating that phosphorylation specifically on S69 regulates late mitotic kinetochore function.

To determine whether any phenotypic consequences result from the dampened oscillations observed in cells unable to phosphorylate Hec1 S69, we quantified chromosome segregation errors in cells expressing both WT- and S69A-Hec1-GFP.
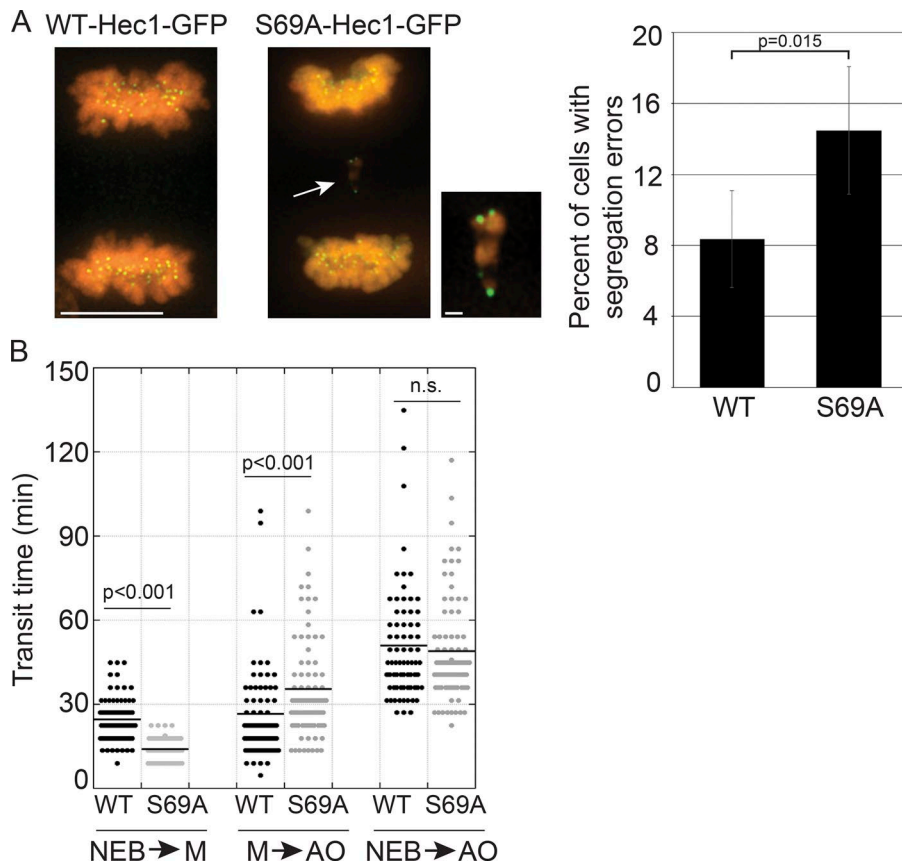
Figure 6. **Inhibition of Hec1 S69 phosphorylation results in chromosome segregation errors and altered mitotic timing. (A)** HeLa Flp-In T-REx cells depleted of endogenous Hec1 and induced to express either WT- or S69A-Hec1-GFP were fixed and scored for segregation errors. Errors included for quantification were lagging anaphase chromosomes and anaphase bridges. Examples of WT- and S69A-Hec1-GFP–expressing cells in anaphase are shown (chromosomes stained with DAPI are in red, and Hec1-GFP is in green). The arrow points to lagging chromosomes; this region is shown magnified to the right. For the quantification, ≥400 cells from four experiments were analyzed. Error bars represent SD. Bars: (main image) 10 µm; (magnified image) 1 µm. **(B)** Quantification of mitotic timing of HeLa Flp-In T-REx cells depleted of endogenous Hec1 and induced to express either WT- or S69A-Hec1-GFP. Mitotic progression was scored from nuclear envelope breakdown (NEB) to metaphase (M) and from metaphase to anaphase onset (AO). Total time in mitosis was scored from nuclear envelope breakdown to anaphase onset. For each condition, ≥75 cells were analyzed.

Doxycycline-inducible HeLa stable cell lines (Flp-In T-REx) were depleted of endogenous Hec1 and induced to express either WT-Hec1-GFP or S69A-Hec1-GFP. Fixed-cell analysis revealed a small but significant increase in chromosome segregation errors: 8% in WT-Hec1-GFP–expressing cells, compared with 14% in S69A-Hec1-GFP–expressing cells (Fig. 6 A). We next determined whether the inability to phosphorylate S69 affected the timing of mitosis. Time-lapse imaging of cells depleted of endogenous Hec1 and expressing either WT- or S69A-Hec1-GFP revealed that the total transit time through mitosis was similar (Fig. 6 B). Interestingly, however, the time from nuclear envelope breakdown to metaphase plate formation was reduced in cells expressing S69A-Hec1-GFP (15 ± 4 min vs. 27 ± 9 min), whereas the time from metaphase to anaphase was extended in the mutant-expressing cells (39 ± 20 min vs. 29 ± 19 min).

Our results thus far point to a model in which Aurora A kinase phosphorylates kinetochore-associated Hec1 throughout mitosis, even when kinetochores are distal from the two spindle poles, where Aurora A resides during mitosis. Inspired by work from Katayama et al. (2008) suggesting that Aurora A could interact with INCENP, we explored the possibility that Aurora A kinase might use INCENP, instead of TPX2, for its localization and activation near kinetochores. We performed pulldown experiments from lysates of bacterial artificial chromosome (BAC) cell lines expressing near-endogenous levels of GFP-tagged INCENP, and the immunoprecipitated INCENP protein complexes were analyzed by mass spectroscopy. In addition to the established binding partners of INCENP, i.e., survivin (BIRC5), borealin (CDCA8), Aurora B, and HP1α (CBX5), we consistently identified Aurora A as an INCENP binding partner

(Fig. 7 A). Aurora A association with INCENP was confirmed by Western blot analysis and did not require microtubules, because Aurora A coprecipitated with INCENP equally well in extracts derived from nocodazole-treated cells and Eg5-inhibited (STLC-treated) cells (Fig. 7 B). Moreover, we mapped the Aurora A binding site in INCENP to a region spanning amino acids 878–897 (Fig. 7 C). In line with this, a fusion protein consisting of LacI and INCENP lacking its N-terminal centromere-targeting domain (LacI-mCherry-ΔCEN-INCENP) recruited Aurora A to a LacO repeat integrated in the short arm of chromosome 1 (Fig. 7 D; Janicki et al., 2004). Interestingly, although endogenous Aurora A was not readily detectable at the centromere region in unperturbed cells, upon overexpression of full-length INCENP, Aurora A was clearly visible at centromeres, colocalizing with INCENP (Fig. 7, E and F). To test whether an endogenous Aurora A–INCENP pool could be responsible for Hec1 S69 phosphorylation, we knocked down INCENP and monitored the phosphorylation status of S69 by immunofluorescence. Depletion of INCENP resulted in ~45% reduction of S69 phosphorylation (Fig. 7 G), a reduction that was more pronounced than what was observed after Aurora B inhibition (Fig. 3 B), suggesting that Aurora A–INCENP contributes to Hec1 S69 phosphorylation. However, the effect of INCENP depletion on S69 phosphorylation was partial compared with Aurora A kinase depletion (Fig. S5 B), and microtubule depolymerization by nocodazole also had a clear effect on S69 phosphorylation (Fig. 2 C). This led us to assess the contribution of the spindle-associated activator of Aurora A, TPX2 (Kufer et al., 2002; Zorba et al., 2014). Indeed, knockdown of TPX2 also reduced S69 phosphorylation (Fig. S5 A). We explain this dual contribution of TPX2 and INCENP to Hec1

S69 phosphorylation by a model in which Aurora A–TPX2 is more dominant in phosphorylating Hec1 S69 in early mitosis when chromosomes are in close proximity to the spindle poles, whereas Aurora A–INCENP maintains this phosphorylation in late mitosis when chromosomes are aligned and away from the poles. Our model predicts that codepletion of INCENP and TPX2 would silence all Aurora A activity toward Hec1 S69. Unfortunately, combined knockdown of INCENP and TPX2 appeared lethal for cells.

## Discussion

Although it is well documented that Aurora A associates with and functions at spindle poles to facilitate spindle pole separation in early mitosis, this kinase has also been implicated in kinetochore function and chromosome congression. Aurora A has been reported to phosphorylate CENP-A, which contributes to chromosome congression through an unknown molecular mechanism (Kunitoku et al., 2003) and has been implicated in the phosphorylation of CENP-E, which is proposed to activate its plus end–directed movement along the microtubule lattice to promote pole-to-spindle equator congression of chromosomes (Kim et al., 2010). Furthermore, Aurora A has been demonstrated to contribute to phosphorylation of Hec1 on pole-proximal kinetochores to promote kinetochore–microtubule turnover (Chmátal et al., 2015; Ye et al., 2015). In the case of CENP-E and Hec1, phosphorylation of these kinetochore substrates by Aurora A was suggested to occur after nuclear envelope breakdown in the vicinity of one of the two spindle poles (Kim et al., 2010; Chmátal et al., 2015; Ye et al., 2015), a logical proposition based on the prominence of Aurora A localization at the poles. In this study, we show that the kinetochore protein Hec1 is phosphorylated by Aurora A not only in early prometaphase, when kinetochores likely encounter a spindle pole, but also in metaphase, when kinetochores are maximally separated from the poles. How does a pole-associated kinase continuously phosphorylate kinetochores during mitosis, even in metaphase? Based on the findings reported in this study, we propose that Aurora A is recruited near the kinetochore region to phosphorylate specific targets during mitosis. We find that Aurora A kinase associates with the centromere protein INCENP during mitosis, which is consistent with a previous study (Katayama et al., 2008) and suggests a possible mechanism for Aurora A localization and activation near the kinetochore region.

We found that inhibition of Aurora A kinase in metaphase, after spindle pole separation had occurred, led to dampened kinetochore movements. Interestingly, mimicking phosphorylation at a single site on the Hec1 tail (i.e., by expression of 8A-S69D-Hec1-GFP or 8A-S55D-Hec1-GFP) restored oscillatory behavior, but not to normal levels (Fig. 5). These data suggest that Aurora A likely has additional roles in facilitating kinetochore–microtubule attachment regulation in metaphase beyond phosphorylating Hec1. These roles might include phosphorylation of other kinetochore targets to affect kinetochore–microtubule attachment stability, or alternatively, they might involve modulating microtubule dynamics, which have been shown to be altered in interphase cells upon Aurora A kinase inhibition (Lorenzo et al., 2009).

Our results demonstrate that pS69 is important for facilitating normal kinetochore–microtubule attachment dynamics, especially during late mitosis, and that preventing phosphoryla-

tion of this site causes a modest increase in segregation errors. We speculate that these errors result from a failure to correct merotelic attachments, whose incidence have been established to increase the rate of anaphase-lagging chromosomes (Cimini et al., 2001). Interestingly, the total transit time through mitosis was unchanged in cells expressing the single S69A mutant, but the time to align chromosomes was shortened. We hypothesize that preventing phosphorylation on a single site in early mitosis likely results in expedited formation of stable kinetochore–microtubule attachments (Zaytsev et al., 2014), and thus, expedited chromosome alignment. Interestingly, once chromosomes have aligned in these cells, the time to anaphase is slightly delayed (Fig. 6). Although the reason for this delay is not clear, it is possible that metaphase chromosome oscillations and their impact on the kinetochore–microtubule interface may influence spindle assembly checkpoint signaling. This remains a topic to be explored in the future. It also remains unclear why this particular site, S69, exists as a target for reversible modification if constitutive phosphorylation is required during all stages of mitosis for normal function and why this site has not evolved into a negatively charged amino acid. In light of its ability to be reversibly modified, it is possible there are conditions that lead to changes in S69 phosphorylation that remain to be revealed. Related to this point, it is interesting that S69 phosphorylation levels remain high in metaphase, whereas nearby target sites including S44 and S55 are largely dephosphorylated. We determined from kinase assays that Aurora A kinase phosphorylates the individual tail domain sites with similar efficiency in vitro, yet in cells, S55 phosphorylation decreases significantly as chromosomes align, but S69 phosphorylation does not. At this time, we are unable to explain this; however, we do not believe that the difference is a result of location within the Hec1 tail because moving S69 to the far N terminus of the tail did not affect its phosphorylation pattern nor its sensitivity to kinase inhibitors (Fig. S3, A–C). It is possible that the sites are differentially dephosphorylated: S69 may be preferentially protected from kinetochore phosphatase activity, or alternatively, S69 may not be targeted by the kinetochore-associated phosphatases that dephosphorylate the other Hec1 tail domain sites, which currently remain unidentified. Future experiments are needed to resolve this important issue.

In contrast with inhibition of Aurora A, we found that inhibition of Aurora B only modestly affected kinetochore oscillations once cells formed a metaphase plate. In agreement with earlier studies, however, we found that inhibition of Aurora B in early mitosis resulted in severe defects in kinetochore–microtubule attachment regulation and severe chromosome segregation errors (not depicted; Kallio et al., 2002; Ditchfield et al., 2003; Hauf et al., 2003; Cimini et al., 2006). Thus, although Aurora B kinase activity may not be essential for kinetochore–microtubule regulation in metaphase, it is critically important in early mitosis to prevent the accumulation of erroneous attachments through phosphorylation of multiple kinetochore targets, including Hec1 (Kelly and Funabiki, 2009; Musacchio, 2011; Carmena et al., 2012; van der Horst and Lens, 2014). Based on our findings, we propose a model for kinetochore–microtubule attachment regulation whereby in early mitosis, both Aurora B and Aurora A phosphorylate Hec1 to promote high levels of kinetochore–microtubule turnover. As chromosomes biorient and kinetochores stably attach to the plus ends of spindle microtubules, Aurora B activity at kinetochores decreases (Lampson and Cheeseman, 2011; Caldas and DeLuca, 2014),
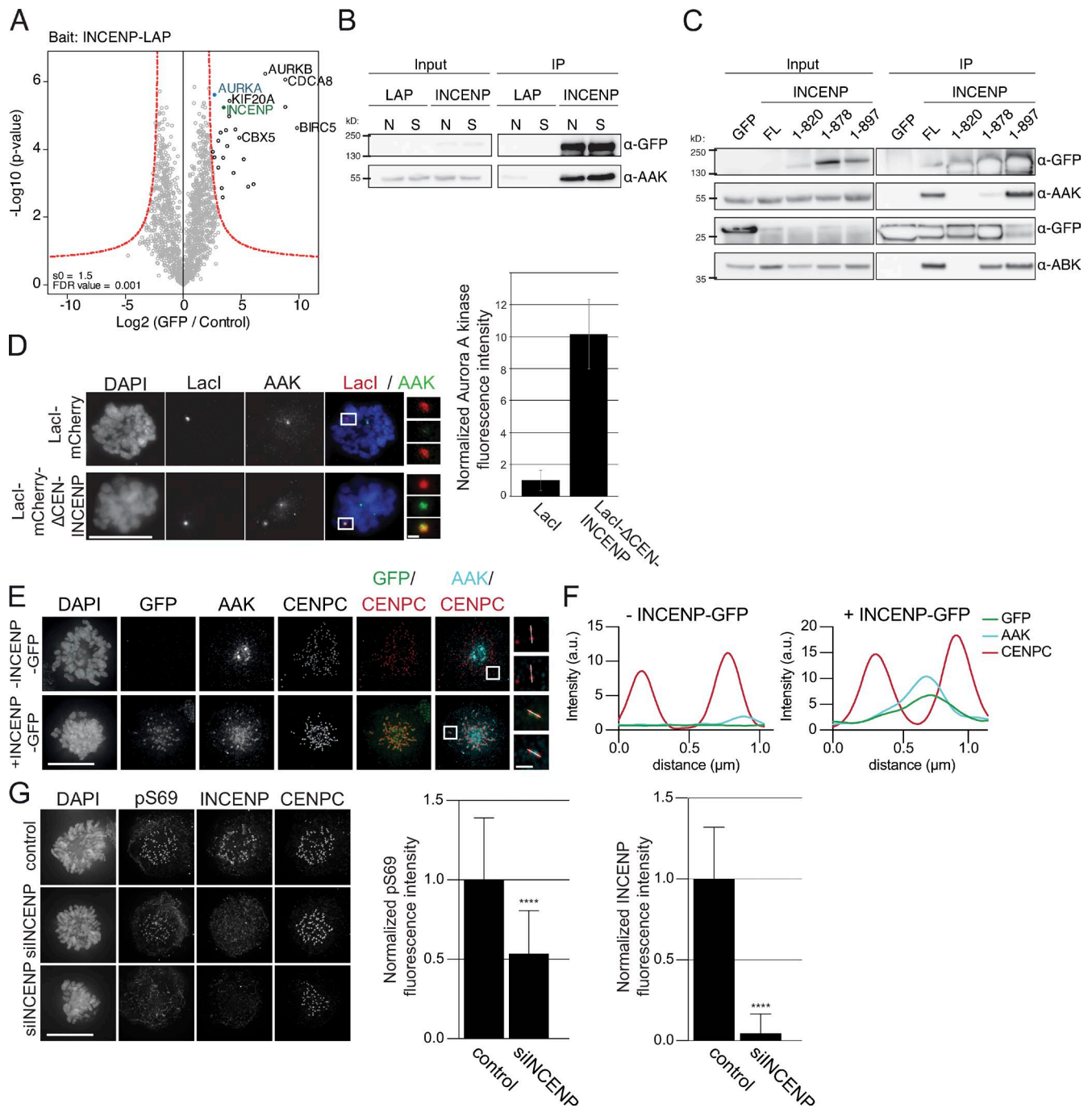
Figure 7. **Aurora A kinase binds and localizes to INCENP. (A)** Volcano plot of quantitative liquid chromatography–tandem mass spectrometry experiments identifying interactors of INCENP. Plotted are the differences in label-free quantification intensity between the INCENP-GFP (right) and control group against the transformed (−$\log_{10}$) p-value of a Student's *t* test. The red line indicates the permutation-based false discovery rate (FDR) threshold (0.001) to correct for multiple testing. **(B)** Western blot analysis of an anti-GFP immunoprecipitation (IP) performed in mitotic cell lysates, using either nocodazole (N) or STLC (S) from HeLa cells expressing either LAP or INCENP-LAP. After SDS-PAGE, the Western blot was probed for GFP and Aurora A kinase (AAK). 10% of input was loaded. **(C)** Western blot analysis of an anti-GFP immunoprecipitation performed in cell lysates from HEK-293T cells transiently expressing either GFP, full-length (FL) INCENP-GFP, or various truncation mutants of INCENP-GFP (1–820, 1–878, and 1–897). The Western blot was probed for GFP and Aurora A kinase and reprobed for Aurora B kinase (ABK). 10% of input was loaded. **(D)** Immunofluorescence images of U2OS cells expressing either LacI-mCherry or LacI-mCherry-ΔCEN-INCENP (a version of INCENP lacking the N-terminal 57 residues; Ainsztein et al., 1998). Cells were immunostained with an Aurora A kinase antibody. Enlarged images show recruitment of Aurora A kinase to the LacI-mCherry-ΔCEN-INCENP spot. Quantification of Aurora A kinase intensity is shown on the right. **(E)** Immunofluorescence images of U2OS cells expressing VSV-INCENP-GFP under a doxycycline-inducible promoter, either noninduced or induced. Cells were immunostained with GFP and Aurora A kinase antibodies. Enlarged images show colocalization of INCENP-GFP and Aurora A kinase upon overexpression of INCENP-GFP. **(F)** Line graphs of kinetochore pairs highlighted in E. **(G)** Immunofluorescence images showing kinetochore localization of pS69 in HeLa cells treated with siRNA to either luciferase (control) or INCENP (siINCENP). Quantification of pS69 and INCENP fluorescence intensity is shown on the right. For pS69 quantification, *n* = 3 experiments of 15–20 cells; for INCENP quantification, *n* = 1 experiment of 15–20 cells. Error bars indicate SD. ****, P < 0.0001; unpaired *t* test. Bars: (main images) 10 µm; (insets) 1 µm.

and sustained kinetochore Hec1 phosphorylation (primarily on S69) is facilitated by Aurora A, most likely bound to INCENP. This low level of Hec1 phosphorylation supports stable kinetochore–microtubule attachment, but importantly, it allows kinetochores to fluidly track the growing and shortening ends of attached microtubules, which is important for error-free chromosome segregation.

## Materials and methods

### Cell culture and generation of cell lines

PtK1 cells were cultured in Ham's F-12 medium supplemented with 10% FBS and 1% antibiotic/antimycotic solution, and maintained at 37°C in 5% $CO_2$. HeLa cells were cultured in DMEM supplemented with 10% FBS and 1% antibiotic/antimycotic solution and maintained at 37°C in 5% $CO_2$. U2OS osteosarcoma cells expressing an ectopic Lac operator array stably integrated into the short arm of chromosome 1 (a gift from S. Janicki; Wistar Institute, Philadelphia, PA; Janicki et al., 2004) were maintained in McCoy's 5A medium supplemented with 10% FBS and 1% antibiotic/antimycotic solution and maintained at 37°C in 5% $CO_2$. Cells were transfected with a LacI-mCherry or LacI-mCherry–ΔCEN-INCENP vector (45236; Addgene; from M. Lampson; Wang et al., 2011) using Lipofectamine 2000 (Thermo Fisher Scientific). HeLa Kyoto cells expressing a BAC transgene of INCENP with a C-terminal localization and affinity purification (LAP) tag were gifts from A.A. Hyman (Poser et al., 2008) and were cultured in DMEM supplemented with 6% FBS, ultraglutamine, and antibiotics and in the presence of 350 µg/ml G418 (Thermo Fisher Scientific). HeLa Kyoto cells expressing only the LAP tag were generated by lentiviral transduction of a p20INDUCER construct (Meerbrey et al., 2011) in which the LAP sequence was cloned. U2OS cells stably expressing tetracycline-inducible INCENP-GFP were described previously (Van der Waal et al., 2012). Protein expression was induced by addition of 1 µg/ml–1 doxycycline for 16 h. HEK293T cells were cultured in DMEM supplemented with 6% FBS, ultraglutamine, and antibiotics and were maintained at 37°C in 5% $CO_2$. Stable cell lines expressing inducible WT-Hec1-GFP, S69A-Hec1-GFP, and domain-swap–Hec1-GFP were generated from a Flp-In T-REx HeLa host cell line (a gift from S. Taylor, University of Manchester, Manchester, England, UK; Tauchman et al., 2015). Cells were grown to 50% confluence in DMEM supplemented with 10% FBS, 1% penicillin/streptomycin, and 2 mM L-glutamine at 37°C in 5% $CO_2$. Cells were transfected with 2.4 µg pOG44 recombinase-containing plasmid and 0.3 µg pcDNA5.FRT.TO-WT-, S69A-, or domain-swap–Hec1-GFP plasmids with Lipofectamine 2000 (Invitrogen). The pcDNA5.FRT.TO-Hec1 plasmids were generated through PCR amplification of WT-, S69A-, or domain-swap–Hec1-GFP fragments and cloned into a pcDNA5.FRT.TO vector through In-Fusion cloning. After 48 h, cells were switched to media containing 100 µg/ml–1 hygromycin (EMD Millipore) and grown in this selection media for 2 wk. Hygromycin-resistant foci were expanded and examined for inducible Hec1-GFP expression. Gene expression was induced with 1 µg/ml–1 doxycycline (Sigma-Aldrich) for 12–24 h.

### Cell treatments and transfections

For live-cell imaging experiments, cells were seeded and imaged in 35-mm glass-bottomed dishes (constructed in-house) and imaged in Leibovitz's L-15 medium (Invitrogen) supplemented with 10% FBS, 7 mM Hepes, and 4.5 g/liter glucose, pH 7.0. For fixed-cell analysis, cells were grown on sterile, acid-washed coverslips in six-well plates. Electroporation was used for Hec1 silence and rescue experiments in PtK1 cells. PtK1 cells were transfected using a nucleofector (Lonza)

electroporator according to the manufacturer's instructions using program T-020 and using the following siRNA and DNA: 8 µl of a 20-µM PtK1-specific Hec1 siRNA labeled with Cy5 (Guimaraes et al., 2008) and 4 µg plasmid DNA. Transfected solutions were added to either 35-mm glass-bottomed dishes or coverslips in six-well plates. Cells were imaged 40–48 h after transfection. HEK293T cells were transfected using the calcium phosphate method. For INCENP siRNA (5′-GGCUUGGCCAGGUGUAUAU-3′), HeLa cells were transfected with 20 nM siRNA using HiPerFect (QIAGEN). All other siRNAs were transfected into HeLa cells using oligofectamine (Thermo Fisher Scientific) as follows: siAAK (5′-CACCUUCGGCAUCCUAAUA-3′) at 80 nM, siTPX2 (5′-GGAUGAACACUUUGAAUUU-3′) at 20 nM, siCENP-E (5′-ACUCUUACUGCUCUCCAGU-3′) at 60 nM, and siHec1 (5′-CCCUGGGUCGUGUCAGGAA-3′) at 160 nM. For silence and rescue experiments in HeLa cells, at the time of siRNA treatment, Hec1-GFP constructs were simultaneously transfected (4 µg) using oligofectamine. For Aurora kinase inhibition experiments, cells were synchronized in early mitosis using a double thymidine block and release. After the second thymidine block, cells were released for 9 h in fresh medium and subsequently treated in the final hour of washout (9–10 h after washout) with either DMSO or kinase inhibitor added at the following concentrations: 2 µM ZM447439 (both HeLa and PtK1 cells), 0.5 µM MLN8054 (HeLa cells), or 1 µM MLN8054 (PtK1 cells; Tocris Bioscience). For analysis of kinetochore oscillations, 10 µM MG132 (Tocris Bioscience) was added in addition to either DMSO or the kinase inhibitors at the concentrations detailed above. For microtubule perturbation experiments, nocodazole was added at 1 µM, or taxol was added at either 50 nM or 10 µM, and these were incubated for 1 h, 5 h, and 30 min respectively.

### Immunofluorescence

Cells were rinsed in 37°C PHEM buffer (60 mM Pipes, 25 mM Hepes, 10 mM EGTA, and 4 mM $MgSO_4$, pH 6.9) and lysed at 37°C for 5 min in freshly prepared lysis buffer (PHEM buffer + 1.0% Triton X-100) containing 100 nM microcystin (Sigma-Aldrich), followed by fixation for 20 min at RT in freshly prepared 4% paraformaldehyde in PHEM buffer (37°C). After fixation, cells were washed 5 × 3 min in PHEM-T (PHEM buffer + 0.1% Triton X-100) and then blocked in 10% boiled donkey serum (BDS) in PHEM for 1 h at RT. Primary antibodies diluted in 5% BDS were added to coverslips and allowed to incubate for 12 h at 4°C. The following primary antibody dilutions were used: mouse anti-Hec1 9G3 at 1:3,000 (Novus Biologicals), human anticentromere antibody at 1:300 (Antibodies, Inc.), DM1α mouse antitubulin at 1:200 (Sigma-Aldrich), rabbit antiphosphorylated Aurora A (pT288) at 1:500 (Cell Signaling Technology), rabbit antiphosphorylated Aurora B (pT232) at 1:1,000, rabbit antiphosphorylated Hec1 Ser44 (pS44) at 1:3,000, rabbit antiphosphorylated Hec1 Ser55 (pS55) at 1:1,000, rabbit antiphosphorylated Hec1 Ser69 (pS69) at 1:3,000, mouse anti-INCENP at 1:1,000 (Abgent), rat anti-GFP at 1:1,000 (ChromoTek), mouse anti–Aurora A at 1:500 (BD), and guinea pig anti–Cenp-C at 1:1,000 (MBL). After primary antibody incubation, cells were rinsed 5 × 3 min in PHEM-T and then incubated for 45 min at RT with secondary antibodies conjugated to either Alexa Fluor 488, Alexa Fluor 568, or Alexa Fluor 647 (Jackson ImmunoResearch Laboratories, Inc.) at 1:300 diluted in 5% BDS. Cells were rinsed 5 × 3 min in PHEM-T, incubated in a solution of 2 ng/ml DAPI diluted in PHEM, rinsed 5 × 3 min, quick rinsed in PHEM, and then mounted onto glass slides in an antifade solution (90% glycerol + 0.5% N-propyl gallate). Coverslips were then sealed with nail polish and stored at 4°C. Double affinity–purified antibodies against Hec1 pS44 and Hec1 pS55 were generated as described previously by DeLuca et al. (2011). Double affinity–purified antibodies against phosphorylated Hec1 Ser69

(pS69) and phosphorylated Aurora B kinase (pT232) were generated at 21st Century Biochemicals. For generation of the Hec1 pS69 antibody, rabbits were immunized with a peptide corresponding to amino acids 64–75 of human Hec1, phosphorylated at S69. For generation of the Aurora B pT232 antibody, rabbits were immunized with a peptide corresponding to amino acids 225–234 of human ABK, phosphorylated at T232. For generation of the Mad2 antibody, full-length PtK1 Mad2 protein was expressed from a pGEX-6P1 plasmid and purified from *Escherichia coli* (mRNA sequence provided by S. Dumont, University of California, San Francisco, San Francisco, CA). Two rabbits were immunized with the Mad2 protein (Rockland Immunochemicals Inc), and antisera from the two injected rabbits were affinity purified against full-length Mad2 protein using a HiTrap-NHS column.

### Imaging and data analysis

All images were acquired on an IX71 inverted microscope (Olympus) incorporated into a DeltaVision Personal DV imaging system (GE Healthcare) using SoftWoRx software (GE Healthcare). For live-cell imaging, cells were maintained at 37°C using an environmental chamber (Precision Control). For mitotic progression experiments, cells were imaged using a 40× 0.75 NA UPlanFl lens (Olympus). For kinetochore oscillation experiments, cells expressing various Hec1-GFP constructs were imaged using a 60× 1.42 NA differential interference contrast Plan Apochromat oil immersion lens (Olympus) with a 1.6 magnification lens inserted into the light path, providing a final magnification of 67 nm/pixel at the camera sensor (CoolSNAP HQ2; Photometrics/Roper Technologies). To ensure oscillation measurements were performed on metaphase cells, mid-to-late prometaphase cell coordinates were marked using SoftWoRx software at the time of inhibitor addition. Approximately 30 min after inhibitor addition, images were acquired every 3 s for 10 min. At each time point, three images were collected in the z axis using a 0.5-µm step size. For all oscillation measurements, only sister kinetochore pairs located in the middle of the spindle were analyzed. Fluorescence intensity of Hec1-GFP at kinetochores was quantified, and only cells expressing GFP within a defined range were used for analysis. For silence and rescue experiments, cells were chosen for analysis only if they were positive for both Hec1-GFP and Cy5-labeled Hec1 siRNA. Kinetochore oscillation movements were tracked on maximum-projection videos using the "track points" function in Metamorph software (Molecular Devices). The deviation from average position was determined using SigmaPlot software (Systat Software) as previously described by Stumpff et al. (2008). For fixed-cell analysis, slides were imaged using the 60× 1.42 NA differential interference contrast Plan Apochromat oil immersion lens (Olympus) and a CoolSNAP HQ2 camera. Images were acquired as z stacks at 0.2-µm intervals. Images were deconvolved using the SoftWoRx enhanced ratio deconvolution algorithm. Fluorescence intensity measurements were performed on nondeconvolved, uncompressed images in MatLab (MathWorks) using a customized program courtesy of X. Wan (Wan et al., 2009). All statistical analyses were performed in SigmaPlot software.

### In vitro kinase assays

For Aurora B kinase assays, a complex of Aurora B (amino acids 60–361) and INCENP (amino acids 790–856) was preactivated by incubation of the kinase (185 nM), in 1× kinase buffer (100 µM ATP, 27.5 mM MgCl$_2$, pH 7.2, 9.17 mM B-glycerol phosphate, 1.83 mM EGTA, 0.37 mM sodium orthovanadate, and 0.37 mM DTT) for 10 min at 30°C. For Aurora A kinase assays, Aurora A (SignalChem) was preactivated by incubation of the kinase (185 nM) in 1× kinase buffer for 10 min at 30°C. Purified NDC80$^{Bonsai}$ was added to the preactivated kinases and allowed to incubate for 20 min at 30°C. Reactions were

terminated by the addition of 5× SDS-PAGE sample buffer. Samples were run on 12% SDS-polyacrylamide gels, transferred to polyvinylidene difluoride membrane (EMD Millipore), and then processed for Western blotting. For phospho-Hec1 staining, blots were incubated with antibodies to Hec1 pS44, pS55, and pS69 at 1:3,000. Primary antibodies were detected using a horseradish peroxidase–conjugated anti–rabbit secondary antibody at 1:10,000 (Jackson ImmunoResearch Laboratories, Inc.) and enhanced chemiluminescence (Thermo Fisher Scientific). Quantifications of band intensities were performed using MetaMorph software. Km values for each phosphorylation site were determined using Prism (GraphPad Software) to simultaneously fit three to five independent experiments per phosphorylation site (17–25 total data points), with a shared Km value but separate signal intensity scale factors for each experiment, using the equation: intensity = scale factor * Hec1/(Km + Hec1). The plots in Fig. 4 B show the normalized mean signals at five representative Hec1 concentrations together with the binding curve calculated from the Prism-derived Km values as listed in Fig. 4 C. Purified NDC80$^{Bonsai}$ was expressed and purified as follows. Glutathione S-transferase (GST)-NDC80$^{Bonsai}$-His6 was provided by A. Musacchio (Max Planck Institute of Molecular Physiology, Dortmund, Germany; Ciferri et al., 2008). NDC80$^{Bonsai}$ constructs were expressed in BL21-DE3 cells by induction with 0.4 mM isopropyl β-D-1-thiogalactopyranoside at 18°C for 16 h. Cells were harvested by centrifugation, and pellets were resuspended in lysis buffer (25 mM Tris, pH 7.6, 300 mM NaCl, and 1 mM EDTA) supplemented with protease inhibitors and DTT. Cell suspensions were sonicated on ice, and cell debris was pelleted by centrifugation at 40,000 rpm for 1 h at 4°C. The supernatant was incubated with glutathione-agarose resin for 1 h at 4°C. Unbound protein was removed by washing, and bound protein was cleaved from GST and the glutathione resin through a 12-h incubation with PreScission Protease (GE Healthcare) at 4°C. Recovered protein was subjected to size-exclusion chromatography on a Superdex 200 HiLoad 16/60 column (GE Healthcare) in lysis buffer supplemented with 5% glycerol and 1 mM DTT. Fractions were pooled and concentrated, and glycerol was added to a final concentration of 20%. Protein aliquots were snap-frozen in liquid nitrogen and stored at −80°C. Fragments of Aurora B kinase and INCENP (plasmids provided by A. Musacchio) were expressed and purified as described by Sessa et al. (2005). In brief, GST-Aurora B$^{60–361}$ was coexpressed with INCENP$^{790–856}$ in *E. coli* (BL21DE3) and purified using glutathione-agarose resin. GST tags were cleaved from the proteins using PreScission Protease while bound to the resin. 20% glycerol was added to the cleaved protein, and aliquots were snap-frozen in liquid nitrogen and stored at −80°C.

### Immunoprecipitation for mass spectrometry and Western blot analysis

HeLa Kyoto cells were synchronized in mitosis by treatment with 20 µM STLC (Tocris Bioscience) or 0.83 µM nocodazole for 16 h (Western blot analysis only) after release from a 24 h thymidine (2.5 mM; Sigma-Aldrich) block. Mitotic cells were collected by mitotic shakeoff and stored at −80°C until use and then were thawed on ice before lysis or lysed immediately. HEK293T cells were treated with 20 µM STLC for 16 h to enrich for mitotic cells, and all cells were collected and lysed immediately. Cells were resuspended in lysis buffer: 50 mM Tris, pH 7.4, 400 mM NaCl, 0.1 mM MgCl$_2$, 0.5% NP-40, 0.24 µM sodium deoxycholate, 2 µM B-glycerol phosphate, 10 mM vanadate, 0.1 mM okadaic acid, protease inhibitors (Complete; Sigma-Aldrich), 12 U/ml MNase (New England Biolabs, Inc.), and 120 µg/ml RNase (Sigma-Aldrich) followed by 1 h incubation at 4°C and 20 min at 37°C. Insoluble material was pelleted by high-speed centrifugation at 4°C. Protein concentration was determined by Bradford assay, and equal protein amounts were added to GFP-Trap beads (ChromoTek) and incubated for 2 h at 4°C

while rotating. For mass spectrometry analysis, three pulldowns were performed per condition (3× technical replicates). Beads were washed three times with lysis buffer and twice with PBS. Beads were either boiled for 5 min in standard SDS sample buffer and subjected to Western blotting according to standard protocol or were further processed for mass spectrometry analysis. Antibodies used for Western blot analysis were rabbit anti-GFP at 1:1,000 (custom made), mouse anti–Aurora B at 1:250 (BD), and rabbit anti–Aurora A at 1:2,000 (Cell Signaling Technology). For immunoprecipitation experiments in Fig. 7, blots were scanned on a chemiluminescence imager IA600 (GE Healthcare).

## Mass spectrometry and data analysis

For mass spectrometry analysis, beads were resuspended in denaturing buffer (100 mM Tris-HCl, 10 mM DTT, and 2 M urea) for 20 min at RT to reduce cysteines, which were subsequently alkylated by iodoacetamide (Sigma-Aldrich) at a final concentration of 50 mM for 20 min in the dark at RT. Proteins were digested with 50 ng/µl modified sequencing grade trypsin (Promega) for 2 h at RT on a shaker, after which the beads were removed by centrifugation for 5 min at 1,500 $g$. After an additional elution of the beads with denaturing buffer, both supernatants were combined, and 10 ng/µl modified sequencing grade trypsin was added and left at RT for 16 h. 10% trifluoroacetic acid was added, and the solution was transferred to C18 columns (EMD Millipore). The bound peptides were eluted from the C18 columns with 98% acetonitrile/0.5% formic acid and dried in a speed-vac, after which they were resuspended in 2% acetonitrile and 0.5% formic acid before loading for liquid chromatography–tandem mass spectrometry. Peptides were separated on an in-house–packed C18 capillary column (75-µm × 25-cm; 3-µm particle size; 100 Å) using a 120-min gradient of 7% to 32% acetonitrile in 0.5% formic acid at a flowrate of 300 nl/min delivered by an Easy nano-LC1000 (Thermo Fisher Scientific) and then were sprayed directly into a LTQ-Orbitrap-Velos mass spectrometer (Thermo Fisher Scientific). Full mass spectrometry scans (from m/z 400–1,750) were acquired with a resolution of R = 60,000 at m/z 400. The 15 most intense ions in the mass spectrometry scan were selected for fragmentation by collision-induced dissociation and measured in the linear ion trap with a target setting of 500 ions. Raw data were analyzed with MaxQuant (version 1.3.0.5; Cox and Mann, 2008) with carbamidomethylation of cysteine set as fixed modification and acetylation of the protein N terminus as well as oxidation of methionine and camthiopropanoyl on lysine set as variable modifications. Up to two missed trypsin cleavages were allowed. Mass tolerance for the precursor ions was set to 10 ppm, and for the tandem mass spectrometry, 0.5 D, and false discovery rate was set to 1%. For label-free quantification, the "LFQ" and "match between runs" options were enabled. Identified proteins were filtered for contaminants and reverse hits, and $t$ test statistics assuming equal variances were applied on log$_2$-transformed label-free quantification intensities using Perseus software (Max Planck Institute of Biochemistry). The mass spectrometry proteomics data have been deposited to the ProteomeXchange Consortium via the PRIDE partner repository with the dataset identifier PXD006892.

## Online supplemental material

Fig. S1 demonstrates phosphospecificity of the pS69 antibody by Western blotting, pS69 kinetochore localization in PtK1 cells, and Mad2 kinetochore localization in cells treated with microtubule poisons. Fig. S2 demonstrates the response of Aurora A and B kinases to Aurora kinase inhibitors. Fig. S3 demonstrates that the location of S69 within the Hec1 tail does not affect levels of S69 phosphorylation during mitosis or its sensitivity to kinase inhibitors. Fig. S4 shows Hec1 phosphospecific antibody recognition in various mutant backgrounds. Fig. S5 demonstrates that Aurora A kinase activity is decreased upon TPX2 depletion.

## References

Ainsztein, A.M., S.E. Kandels-Lewis, A.M. Mackay, and W.C. Earnshaw. 1998. INCENP centromere and spindle targeting: identification of essential conserved motifs and involvement of heterochromatin protein HP1. *J. Cell Biol.* 143:1763–1774. https://doi.org/10.1083/jcb.143.7.1763

Barr, A.R., and F. Gergely. 2007. Aurora-A: the maker and breaker of spindle poles. *J. Cell Sci.* 120:2987–2996. https://doi.org/10.1242/jcs.013136

Biggins, S., F.F. Severin, N. Bhalla, I. Sassoon, A.A. Hyman, and A.W. Murray. 1999. The conserved protein kinase Ipl1 regulates microtubule binding to kinetochores in budding yeast. *Genes Dev.* 13:532–544. https://doi.org/10.1101/gad.13.5.532

Caldas, G.V., and J.G. DeLuca. 2014. KNL1: bringing order to the kinetochore. *Chromosoma.* 123:169–181. https://doi.org/10.1007/s00412-013-0446-5

Caldas, G.V., K.F. DeLuca, and J.G. DeLuca. 2013. KNL1 facilitates phosphorylation of outer kinetochore proteins by promoting Aurora B kinase activity. *J. Cell Biol.* 203:957–969. https://doi.org/10.1083/jcb.201306054

Carmena, M., M. Wheelock, H. Funabiki, and W.C. Earnshaw. 2012. The chromosomal passenger complex (CPC): from easy rider to the godfather of mitosis. *Nat. Rev. Mol. Cell Biol.* 13:789–803. https://doi.org/10.1038/nrm3474

Cheeseman, I.M., and A. Desai. 2008. Molecular architecture of the kinetochore-microtubule interface. *Nat. Rev. Mol. Cell Biol.* 9:33–46. https://doi.org/10.1038/nrm2310

Cheeseman, I.M., J.S. Chappie, E.M. Wilson-Kubalek, and A. Desai. 2006. The conserved KMN network constitutes the core microtubule-binding site of the kinetochore. *Cell.* 127:983–997. https://doi.org/10.1016/j.cell.2006.09.039

Chmátal, L., K. Yang, R.M. Schultz, and M.A. Lampson. 2015. Spatial regulation of kinetochore microtubule attachments by destabilization at spindle poles in Meiosis I. *Curr. Biol.* 25:1835–1841. https://doi.org/10.1016/j.cub.2015.05.013

Ciferri, C., S. Pasqualato, E. Screpanti, G. Varetti, S. Santaguida, G. Dos Reis, A. Maiolica, J. Polka, J.G. De Luca, P. De Wulf, et al. 2008. Implications for kinetochore-microtubule attachment from the structure of an engineered Ndc80 complex. *Cell.* 133:427–439. https://doi.org/10.1016/j.cell.2008.03.020

Cimini, D., B. Howell, P. Maddox, A. Khodjakov, F. Degrassi, and E.D. Salmon. 2001. Merotelic kinetochore orientation is a major mechanism of aneuploidy in mitotic mammalian tissue cells. *J. Cell Biol.* 153:517–527. https://doi.org/10.1083/jcb.153.3.517

Cimini, D., X. Wan, C.B. Hirel, and E.D. Salmon. 2006. Aurora kinase promotes turnover of kinetochore microtubules to reduce chromosome segregation errors. *Curr. Biol.* 16:1711–1718. https://doi.org/10.1016/j.cub.2006.07.022

Cox, J., and M. Mann. 2008. MaxQuant enables high peptide identification rates, individualized p.p.b.-range mass accuracies and proteome-wide protein quantification. *Nat. Biotechnol.* 26:1367–1372. https://doi.org/10.1038/nbt.1511

DeLuca, J.G., and A. Musacchio. 2012. Structural organization of the kinetochore-microtubule interface. *Curr. Opin. Cell Biol.* 24:48–56. https://doi.org/10.1016/j.ceb.2011.11.003

DeLuca, J.G., W.E. Gall, C. Ciferri, D. Cimini, A. Musacchio, and E.D. Salmon. 2006. Kinetochore microtubule dynamics and attachment stability are regulated by Hec1. *Cell.* 127:969–982. https://doi.org/10.1016/j.cell.2006.09.047

DeLuca, K.F., S.M. Lens, and J.G. DeLuca. 2011. Temporal changes in Hec1 phosphorylation control kinetochore-microtubule attachment stability during mitosis. *J. Cell Sci.* 124:622–634. https://doi.org/10.1242/jcs.072629

Derry, W.B., L. Wilson, and M.A. Jordan. 1995. Substoichiometric binding of taxol suppresses microtubule dynamics. *Biochemistry.* 34:2203–2211. https://doi.org/10.1021/bi00007a014

Ditchfield, C., V.L. Johnson, A. Tighe, R. Ellston, C. Haworth, T. Johnson, A. Mortlock, N. Keen, and S.S. Taylor. 2003. Aurora B couples chromosome alignment with anaphase by targeting BubR1, Mad2, and Cenp-E to kinetochores. *J. Cell Biol.* 161:267–280. https://doi.org/10.1083/jcb.200208091

Ducat, D., and Y. Zheng. 2004. Aurora kinases in spindle assembly and chromosome segregation. *Exp. Cell Res.* 301:60–67. https://doi.org/10.1016/j.yexcr.2004.08.016

Guimaraes, G.J., Y. Dong, B.F. McEwen, and J.G. Deluca. 2008. Kinetochore-microtubule attachment relies on the disordered N-terminal tail domain of Hec1. *Curr. Biol.* 18:1778–1784. https://doi.org/10.1016/j.cub.2008.08.012

Hans, F., D.A. Skoufias, S. Dimitrov, and R.L. Margolis. 2009. Molecular distinctions between Aurora A and B: a single residue change transforms Aurora A into correctly localized and functional Aurora B. *Mol. Biol. Cell.* 20:3491–3502. https://doi.org/10.1091/mbc.E09-05-0370

Hauf, S., R.W. Cole, S. LaTerra, C. Zimmer, G. Schnapp, R. Walter, A. Heckel, J. van Meel, C.L. Rieder, and J.M. Peters. 2003. The small molecule Hesperadin reveals a role for Aurora B in correcting kinetochore-microtubule attachment and in maintaining the spindle assembly checkpoint. *J. Cell Biol.* 161:281–294. https://doi.org/10.1083/jcb.200208092

Hoar, K., A. Chakravarty, C. Rabino, D. Wysong, D. Bowman, N. Roy, and J.A. Ecsedy. 2007. MLN8054, a small-molecule inhibitor of Aurora A, causes spindle pole and chromosome congression defects leading to aneuploidy. *Mol. Cell. Biol.* 27:4513–4525. https://doi.org/10.1128/MCB.02364-06

Hochegger, H., N. Hégarat, and J.B. Pereira-Leal. 2013. Aurora at the pole and equator: overlapping functions of Aurora kinases in the mitotic spindle. *Open Biol.* 3:120185. https://doi.org/10.1098/rsob.120185

Janicki, S.M., T. Tsukamoto, S.E. Salghetti, W.P. Tansey, R. Sachidanandam, K.V. Prasanth, T. Ried, Y. Shav-Tal, E. Bertrand, R.H. Singer, and D.L. Spector. 2004. From silencing to gene expression: real-time analysis in single cells. *Cell.* 116:683–698. https://doi.org/10.1016/S0092-8674(04)00171-0

Jordan, M.A., D. Thrower, and L. Wilson. 1992. Effects of vinblastine, podophyllotoxin and nocodazole on mitotic spindles. Implications for the role of microtubule dynamics in mitosis. *J. Cell Sci.* 102:401–416.

Jordan, M.A., R.J. Toso, D. Thrower, and L. Wilson. 1993. Mechanism of mitotic block and inhibition of cell proliferation by taxol at low concentrations. *Proc. Natl. Acad. Sci. USA.* 90:9552–9556. https://doi.org/10.1073/pnas.90.20.9552

Kallio, M.J., M.L. McCleland, P.T. Stukenberg, and G.J. Gorbsky. 2002. Inhibition of aurora B kinase blocks chromosome segregation, overrides the spindle checkpoint, and perturbs microtubule dynamics in mitosis. *Curr. Biol.* 12:900–905. https://doi.org/10.1016/S0960-9822(02)00887-4

Katayama, H., K. Sasai, M. Kloc, B.R. Brinkley, and S. Sen. 2008. Aurora kinase-A regulates kinetochore/chromatin associated microtubule assembly in human cells. *Cell Cycle.* 7:2691–2704. https://doi.org/10.4161/cc.7.17.6460

Kelly, A.E., and H. Funabiki. 2009. Correcting aberrant kinetochore microtubule attachments: an Aurora B-centric view. *Curr. Opin. Cell Biol.* 21:51–58. https://doi.org/10.1016/j.ceb.2009.01.004

Kettenbach, A.N., D.K. Schweppe, B.K. Faherty, D. Pechenick, A.A. Pletnev, and S.A. Gerber. 2011. Quantitative phosphoproteomics identifies substrates and functional modules of Aurora and Polo-like kinase activities in mitotic cells. *Sci. Signal.* 4:rs5. https://doi.org/10.1126/scisignal.2001497

Kim, Y., A.J. Holland, W. Lan, and D.W. Cleveland. 2010. Aurora kinases and protein phosphatase 1 mediate chromosome congression through regulation of CENP-E. *Cell.* 142:444–455. https://doi.org/10.1016/j.cell.2010.06.039

Kufer, T.A., H.H. Silljé, R. Körner, O.J. Gruss, P. Meraldi, and E.A. Nigg. 2002. Human TPX2 is required for targeting Aurora-A kinase to the spindle. *J. Cell Biol.* 158:617–623. https://doi.org/10.1083/jcb.200204155

Kunitoku, N., T. Sasayama, T. Marumoto, D. Zhang, S. Honda, O. Kobayashi, K. Hatakeyama, Y. Ushio, H. Saya, and T. Hirota. 2003. CENP-A phosphorylation by Aurora-A in prophase is required for enrichment of Aurora-B at inner centromeres and for kinetochore function. *Dev. Cell.* 5:853–864. https://doi.org/10.1016/S1534-5807(03)00364-2

Lampson, M.A., and I.M. Cheeseman. 2011. Sensing centromere tension: Aurora B and the regulation of kinetochore function. *Trends Cell Biol.* 21:133–140. https://doi.org/10.1016/j.tcb.2010.10.007

Lampson, M.A., K. Renduchitala, A. Khodjakov, and T.M. Kapoor. 2004. Correcting improper chromosome-spindle attachments during cell division. *Nat. Cell Biol.* 6:232–237. https://doi.org/10.1038/ncb1102

Li, S., Z. Deng, J. Fu, C. Xu, G. Xin, Z. Wu, J. Luo, G. Wang, S. Zhang, B. Zhang, et al. 2015. Spatial Compartmentalization Specializes the Function of Aurora A and Aurora B. *J. Biol. Chem.* 290:17546–17558. https://doi.org/10.1074/jbc.M115.652453

Liu, D., G. Vader, M.J. Vromans, M.A. Lampson, and S.M. Lens. 2009. Sensing chromosome bi-orientation by spatial separation of aurora B kinase from kinetochore substrates. *Science.* 323:1350–1353. https://doi.org/10.1126/science.1167000

Lorenzo, C., Q. Liao, M.A. Hardwicke, and B. Ducommun. 2009. Pharmacological inhibition of aurora-A but not aurora-B impairs interphase microtubule dynamics. *Cell Cycle.* 8:1733–1737. https://doi.org/10.4161/cc.8.11.8617

Manfredi, M.G., J.A. Ecsedy, K.A. Meetze, S.K. Balani, O. Burenkova, W. Chen, K.M. Galvin, K.M. Hoar, J.J. Huck, P.J. LeRoy, et al. 2007. Antitumor activity of MLN8054, an orally active small-molecule inhibitor of Aurora A kinase. *Proc. Natl. Acad. Sci. USA.* 104:4106–4111. https://doi.org/10.1073/pnas.0608798104

Meerbrey, K.L., G. Hu, J.D. Kessler, K. Roarty, M.Z. Li, J.E. Fang, J.I. Herschkowitz, A.E. Burrows, A. Ciccia, T. Sun, et al. 2011. The pIND UCER lentiviral toolkit for inducible RNA interference in vitro and in vivo. *Proc. Natl. Acad. Sci. USA.* 108:3665–3670. https://doi.org/10.1073/pnas.1019736108

Musacchio, A. 2011. Spindle assembly checkpoint: the third decade. *Philos. Trans. R. Soc. Lond. B Biol. Sci.* 366:3595–3604. https://doi.org/10.1098/rstb.2011.0072

Poser, I., M. Sarov, J.R. Hutchins, J.K. Hériché, Y. Toyoda, A. Pozniakovsky, D. Weigl, A. Nitzsche, B. Hegemann, A.W. Bird, et al. 2008. BAC TransgeneOmics: a high-throughput method for exploration of protein function in mammals. *Nat. Methods.* 5:409–415. https://doi.org/10.1038/nmeth.1199

Sarangapani, K.K., and C.L. Asbury. 2014. Catch and release: how do kinetochores hook the right microtubules during mitosis? *Trends Genet.* 30:150–159. https://doi.org/10.1016/j.tig.2014.02.004

Schaar, B.T., G.K. Chan, P. Maddox, E.D. Salmon, and T.J. Yen. 1997. CENP-E function at kinetochores is essential for chromosome alignment. *J. Cell Biol.* 139:1373–1382. https://doi.org/10.1083/jcb.139.6.1373

Sessa, F., M. Mapelli, C. Ciferri, C. Tarricone, L.B. Areces, T.R. Schneider, P.T. Stukenberg, and A. Musacchio. 2005. Mechanism of Aurora B activation by INCENP and inhibition by hesperadin. *Mol. Cell.* 18:379–391. https://doi.org/10.1016/j.molcel.2005.03.031

Silva, V.C., and L. Cassimeris. 2013. Stathmin and microtubules regulate mitotic entry in HeLa cells by controlling activation of both Aurora kinase A and Plk1. *Mol. Biol. Cell.* 24:3819–3831. https://doi.org/10.1091/mbc.E13-02-0108

Stumpff, J., G. von Dassow, M. Wagenbach, C. Asbury, and L. Wordeman. 2008. The kinesin-8 motor Kif18A suppresses kinetochore movements to control mitotic chromosome alignment. *Dev. Cell.* 14:252–262. https://doi.org/10.1016/j.devcel.2007.11.014

Tanaka, T.U., N. Rachidi, C. Janke, G. Pereira, M. Galova, E. Schiebel, M.J. Stark, and K. Nasmyth. 2002. Evidence that the Ipl1-Sli15 (Aurora kinase-INCENP) complex promotes chromosome bi-orientation by

altering kinetochore-spindle pole connections. *Cell.* 108:317–329. https://doi.org/10.1016/S0092-8674(02)00633-5

Tauchman, E.C., F.J. Boehm, and J.G. DeLuca. 2015. Stable kinetochore-microtubule attachment is sufficient to silence the spindle assembly checkpoint in human cells. *Nat. Commun.* 6:10036. https://doi.org/10.1038/ncomms10036

van der Horst, A., and S.M. Lens. 2014. Cell division: control of the chromosomal passenger complex in time and space. *Chromosoma.* 123:25–42. https://doi.org/10.1007/s00412-013-0437-6

Van der Waal, M.S., A.T. Saurin, M.J. Vromans, M. Vleugel, C. Wurzenberger, D.W. Gerlich, R.H. Medema, G.J. Kops, and S.M. Lens. 2012. Mps1 promotes rapid centromere accumulation of Aurora B. *EMBO Rep.* 9:847–854. https://doi.org/10.1038/embor.2012.93

Wan, X., R.P. O'Quinn, H.L. Pierce, A.P. Joglekar, W.E. Gall, J.G. DeLuca, C.W. Carroll, S.T. Liu, T.J. Yen, B.F. McEwen, et al. 2009. Protein architecture of the human kinetochore microtubule attachment site. *Cell.* 137:672–684. https://doi.org/10.1016/j.cell.2009.03.035

Wang, E., E.R. Ballister, and M.A. Lampson. 2011. Aurora B dynamics at centromeres create a diffusion-based phosphorylation gradient. *J. Cell Biol.* 194:539–549. https://doi.org/10.1083/jcb.20110304421844210

Wood, K.W., R. Sakowicz, L.S. Goldstein, and D.W. Cleveland. 1997. CENP-E is a plus end-directed kinetochore motor required for metaphase chromosome alignment. *Cell.* 91:357–366. https://doi.org/10.1016/S0092-8674(00)80419-5

Ye, A.A., J. Deretic, C.M. Hoel, A.W. Hinman, D. Cimini, J.P. Welburn, and T.J. Maresca. 2015. Aurora A Kinase Contributes to a Pole-Based Error Correction Pathway. *Curr. Biol.* 25:1842–1851. https://doi.org/10.1016/j.cub.2015.06.021

Zaytsev, A.V., L.J. Sundin, K.F. DeLuca, E.L. Grishchuk, and J.G. DeLuca. 2014. Accurate phosphoregulation of kinetochore-microtubule affinity requires unconstrained molecular interactions. *J. Cell Biol.* 206:45–59. https://doi.org/10.1083/jcb.201312107

Zaytsev, A.V., J.E. Mick, E. Maslennikov, B. Nikashin, J.G. DeLuca, and E.L. Grishchuk. 2015. Multisite phosphorylation of the NDC80 complex gradually tunes its microtubule-binding affinity. *Mol. Biol. Cell.* 15:1829–1844. https://doi.org/10.1091/mbc.E14-11-1539

Zorba, A., V. Buosi, S. Kutter, N. Kern, F. Pontiggia, Y.J. Cho, and D. Kern. 2014. Molecular mechanism of Aurora A kinase autophosphorylation and its allosteric activation by TPX2. *eLife.* 3:e02667. https://doi.org/10.7554/eLife.02667